

**MEASUREMENT OF MATERIAL Q IN RAYLEIGH WAVES WITH
A LASER BASED ACOUSTIC SPECTROMETER**

A Thesis
Presented to
The Academic Faculty

by

Eric W. Massey

In Partial Fulfillment
of the Requirements for the Degree
Masters of Science in Electrical and Computer Engineering in the
School of Electrical and Computer Engineering

Georgia Institute of Technology
December 2006

COPYRIGHT 2006 BY ERIC W. MASSEY

**MEASUREMENT OF MATERIAL Q IN RAYLEIGH WAVES WITH
A LASER BASED ACOUSTIC SPECTROMETER**

Approved by:

Dr. William D. Hunt Advisor
School of Electrical and Computer Engineering
Georgia Institute of Technology

Dr. Ali Adibi
School of Electrical and Computer Engineering
Georgia Institute of Technology

Dr. Steve J. Kenney
School of Electrical and Computer Engineering
Georgia Institute of Technology

Date Approved: November 20, 2006

ACKNOWLEDGEMENTS

I would first like to begin by thanking my advisor Dr. Bill Hunt for giving me the opportunity to join the MAG lab and have the pleasure to work with some of the finest students I have met during my 5+ years at Georgia Tech. I am grateful for his guidance on this thesis as well as the input he has always been willing to provide for life in general. I have also thoroughly enjoyed his unique sense of humor which has made this experience much more entertaining. I would also like to thank Dr. Ali Adibi and Saeed Mohammadi for their assistance with the laser probe and general suggestions regarding my work. Their assistance has been invaluable to me. I want to thank Dr. Larry Jacobs for the discussions we had and for introducing me to the acoustic Kramers-Kronig relations. I also want to thank James Steinberg in the senior design lab for helping me with some of my questions during the assembly and modification phases of the laser probe. I also want to express my appreciation for Dr. Steve Kenney for being on my thesis committee. Lastly, I would like to thank Dr. Alex Maznev and Yun Li of Phillips AMS for their donation of the laser probe to our lab and for their assistance along the way.

To the guys in the MAG lab (past and present)¹, it has truly been an honor to work with all of you. I have enjoyed getting to know you and consider you all my friends as well as coworkers. From science and engineering, to politics and religion, to landing on the moon or not landing on the moon, the discussions we have had together have been

¹ Ryan Westafer, Tony Dickherber, Chris Corso, Farasat Munir, John Perng, Adam Wathen, George Yu, Dr. “Sangstrom” Lee, and Dr. Desmond Stubbs

some of the most stimulating and entertaining I have had while at Tech. I would also like to thank Ryan Westafer individually for being a fantastic partner in our endeavors to bring the laser probe online.

To my family, friends, and teammates, not already mentioned above, your support has been tremendous and my sanity would not still be intact with out all of you. I want to thank Coach Bradd and Coach Hinsdale for not only giving me the opportunity to compete on the track and field team, but also for giving me the flexibility to pursue my academic goals as well. I would also like to thank my teammates, especially the throwers, who I spent a part of every day with for the past two seasons for their support and frequent entertainment. You guys are all very talented and I look forward to seeing you all dominate the ACC conference. To my many friends I have made at Tech, thank you for being a part of my life and rest assured I would go to bat for any and all of you any day of the week. I would especially like to thank Kelsey and Tomasz for putting up with me as a roommate for the past 5 years and Adrienne for her constant support. Lastly, I want to thank Mom, Dad, Diana, and the rest of my family for their love and support.

TABLE OF CONTENTS

	Page
ACKNOWLEDGEMENTS	iii
LIST OF TABLES	vii
LIST OF FIGURES	viii
LIST OF SYMBOLS AND ABBREVIATIONS	x
SUMMARY	xi
<u>CHAPTER</u>	
1 Introduction	1
Laser Probe Overview	1
Dispersion Data and Kramers-Kronig Calculations	3
Experimental Procedure	4
2 Background on Acoustics in Solids	5
Surface Acoustic Wave Background	5
Material Q Background	9
3 Laser Probe	13
Laser Probe Design	13
Preparatory work	16
Physics of Operation	19
4 Kramers-Kronig Relations	24
Derivation of the Kramers-Kronig Relations	25
Derivation of the non-local Kramers-Kronig Approximations	27
5 Experimental Procedure	34
Experimental Procedure	34

Acoustic Data Acquisition	38
Mathematical Analysis Software	39
6 Experimental Data and Analysis of Results	42
Experimental vs. Theoretical Data	43
Material Q over direction	47
7 Conclusion	49
APPENDIX A: Matlab Code Used for Analysis of Dispersion Data	50
APPENDIX B: Graphical User Interface Screen Shots	58
REFERENCES	60

LIST OF TABLES

	Page
Table 5.1: Corresponding Wavelengths for each Phase Mask setting	38

LIST OF FIGURES

	Page
Figure 2.1: Elliptical Polarization of Rayleigh Waves	6
Figure 2.2: Profile of Ocean Waves versus Rayleigh Waves	6
Figure 2.3: Symmetric versus Anti-Symmetric Lamb Waves	7
Figure 2.4: Exact versus approximate solution to the Rayleigh wave characteristic equation	8
Figure 2.5: Particle velocity and displacement field distributions and	9
Figure 3.1: The laser probe optics head and corresponding schematic	13
Figure 3.2: The optical path of the excitation beam	14
Figure 3.3: The optical path of the probe beam	15
Figure 3.4: Binary Phase Mask Diffraction	20
Figure 3.5: Melted Excitation Pattern Image	21
Figure 3.6: Waveform before “Cleaning”	22
Figure 3.7: Waveform after “Cleaning”	22
Figure 4.1: Infinite Half-Circle Counter	27
Figure 4.2: Comparison between Acoustic and Electromagnetic Equations	27
Figure 4.3: The singularity about $x=0$ for the function $\ln[\coth(x /2)]$	31
Figure 5.1: The aluminum plate used in wafer alignment	35
Figure 5.2: The angles labeled on the motor stage	35
Figure 5.3: The excitation and probe beam dependency on alignment	37
Figure 5.4: Pre-filtered and Post-filtered measured waveforms	40
Figure 5.5: A cleaned up FFT of a Post-filtered waveform	41
Figure 6.1: Theoretical vs. Experimental Dispersion Curve	44
Figure 6.2: Theoretical vs. Experimental Attenuation Curve	45

Figure 6.3: Theoretical vs. Experimental Material Q Curve	46
Figure 6.4: Dispersion, Attenuation, and Material Q for the (100) direction	48
Figure 6.5: Dispersion, Attenuation, and Material Q for 30 degrees off of (100)	48
Figure A.1: Matlab code for the function DispersionCurves.m	50
Figure A.2: Matlab code for the function WaveData.m	53
Figure A.3: A sample wave data file	57
Figure B.1: GUI Screen capture prior to surface melting	58
Figure B.2: GUI Screen capture after surface melting	59

LIST OF SYMBOLS AND ABBREVIATIONS

MAG	Microelectronic Acoustics Group
CAN	Controller Area Network
FDTD	Finite-Difference Tim-Domain
Phillips AMS	Phillips Advanced Metrology Systems

SUMMARY

I have developed a method which can quickly measure the Rayleigh wave Q for a test material using a minimally invasive laser probe. The probe was donated to our lab by Dr. Alex Maznev at Phillips AMS in Natick, Ma. The machine was originally used to measure ultra thin film metal thicknesses; however we have utilized it to suit our needs. The optics head relies on a technique known as the transient grating method to generate a dispersion curve. This dispersion curve is then operated on by a local approximation for the Kramers-Kronig relations. The Kramers-Kronig relations for acoustic waves relate the real and imaginary parts of the dynamic compressibility to one another. The real part of the compressibility relates to the phase velocity of the wave and the imaginary part relates to the attenuation. Once the attenuation for the corresponding range of frequencies is determined the last step is to apply both the dispersion data and the attenuation data to the material Q equation to find Q over a range of frequencies. My thesis discusses the design of the machine, the theory behind the Kramers-Kronig relations and surface acoustic waves, the experimental procedure, and lastly results generated by the technique.

CHAPTER 1

INTRODUCTION

Many RF filters, biosensors, and other microelectronic devices rely on surface acoustic waves for operation. Surface acoustic wave resonators especially rely on one figure of merit, Material Q. Material Q is the ratio of energy stored per cycle divided by energy lost per cycle as the acoustic wave propagates within the medium. The higher the Material Q, the higher the upper limit for the total Q of a resonator or other such acoustic wave device.

There is limited information available for material Q values of Rayleigh waves in literature and in texts. The motivation of this thesis is to be able to rapidly measure the material Q of a given substrate, using minimally invasive techniques. In less than one minute the material Q of a solid can be measured without the need for an IDT to be fabricated on the surface. This thesis describes a novel method we have developed in order to measure material Q based on just the dispersion data. This is done by applying the Kramers-Kronig relationship to the dispersion data over frequency and calculating the corresponding attenuation. Typically in the study of acoustics and geology, attenuation data is first gathered and the Kramers-Kronig relationship is used to calculate the dispersion data. [4, 5] This technique has the added benefit of calculating material Q from one set of data, rather than having to measure the dispersion and attenuation before the calculation can be done.

1.1 Laser Probe Overview

Chapter 3 of this thesis will discuss the details of the laser probe. The laser probe used in the experiment was kindly donated by Alex A. Maznev at Phillips AMS in Natick,

MA. The donated optics head was part of a system called the Impulse 300 which costs in excess of \$1,000,000. The optics head and motor stage that was donated to our lab totaled a value in excess of \$180,000. The entire system was originally designed for thickness measurements of ultra thin metal films on CMOS circuits. This metrology tool has found much success in the semiconductor industry the measurements were done using a method known as Transient Grating (TG) or Impulsive Stimulated Thermal Scattering (ISTS). A diffraction grating is used to diffract an excitation beam. The two first order diffractions of the beam pass through a set of lenses that recombine the beams at the surface of a test wafer. The angle of recombination dictates the fringe pattern which in turn dictates the wavelength of the acoustic wave generated. The resulting surface acoustic wave is then measured by an IR probe beam which is shone directly on the “ripple” of the surface. The first order diffracted beam is then detected by a high speed avalanche photo receiver and that signal is in turn output to a 2 Gb/s LeCroy Oscilloscope.

The resulting signal can then be analyzed by MATLAB to extract information about the wave. I perform an FFT on the signal to determine the frequency of the propagating wave. The phase velocity of the wave is then calculated using the familiar equation:

$$V_s = \lambda \cdot f \quad (1.1)$$

where λ is the wavelength of the SAW wave and f is the frequency of the wave. The resultant signal can also be operated on in other ways to provide data useful for calculating material Q for different substances. A detailed description regarding the nature of acoustic waves, more specifically Rayleigh waves will be given in chapter 2.

1.2 Dispersion Data and Kramers-Kronig Calculations

The dispersion curve can be created from the collected velocities at different wavelengths. The dispersion curve is plotted over frequency to view the trend in the change of acoustic phase velocity as the frequency increases. The dispersion data is then operated on by a set of approximations based off the Kramers-Kronig relationship. The Kramers-Kronig relationship was first developed to relate the real and imaginary part of a complex wave number. Essentially, this relationship allows dispersion data to be translated into attenuation data for the corresponding frequencies and vice versa. Unfortunately, advanced knowledge of a point in the destination data set is necessary for the relationship. To mitigate the problem a set of approximations have been developed to allow for dispersion data that is relatively constant over a small range of frequencies to be used to find the corresponding attenuation data. [5, 6]

After the dispersion data is gathered and the corresponding attenuation data has been calculated material Q can be calculated for the corresponding range of frequencies. The formula used for the final calculation of Q is:

$$Q = \frac{\omega}{2 \cdot \alpha \cdot V_a} \quad (1.2)$$

where ω is the angular frequency, α is the attenuation coefficient and V_a is the velocity of the acoustic wave. [3] Further discussion regarding material Q will be held in chapter 2. A derivation of the Kramers-Kronig relations as well as the approximations used in this experiment will be presented in Chapter 4.

1.3 Experimental Procedure

The fifth chapter will detail the steps needed to perform the experiment. First, the preliminary preparations including wafer preparation, setting up the laser probe, properly aligning the system and other steps will be discussed. Second, the actual control of the machine and operation of the system will be discussed. Last, a description of the Labview based dispersion curve program and the MATLAB mathematical analysis software will both be presented to better explain the code.

CHAPTER 2

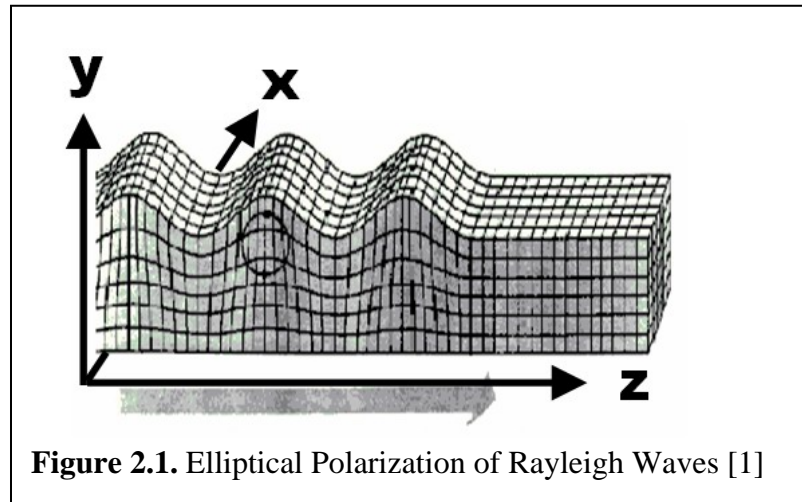
BACKGROUND ON SURFACE ACOUSTIC WAVES IN SOLIDS

This chapter will provide the necessary background information regarding surface acoustic waves in solids. This chapter is relevant to this thesis because the acoustic waves generated by the laser probe are surface modes. This chapter will focus on the physics of first order surface waves, known as Rayleigh waves, since they are the waves of study in this thesis. Higher order modes, such as Sezawa modes, can be generated by the laser probe when a thick enough surface layer is present. In my experiment however, the top layer is kept acoustically thin enough that these modes are not present.

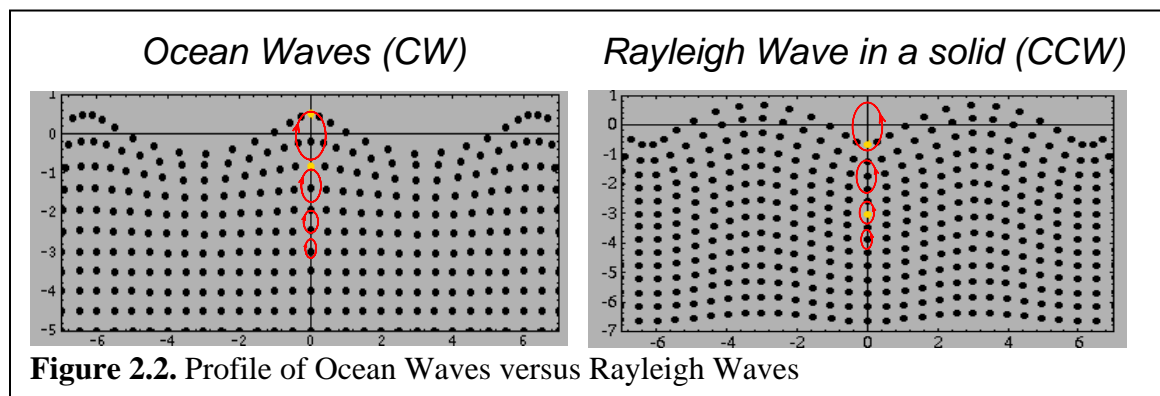
This section will be divided into two parts, the first discussing Rayleigh Wave physics and propagation, the next discussing material Q for acoustic waves, primarily Rayleigh waves. Discovered in 1887 by Lord Rayleigh, Rayleigh waves are surface acoustic waves that are confined to the surface of a medium. The energy of the wave decays exponentially into the substrate and is typically non-existent at a depth on the order of a wavelength. Material Q for Rayleigh waves is an important figure of merit since it is a necessary parameter used by engineers when designing acoustic devices.

2.1 Rayleigh Wave Background

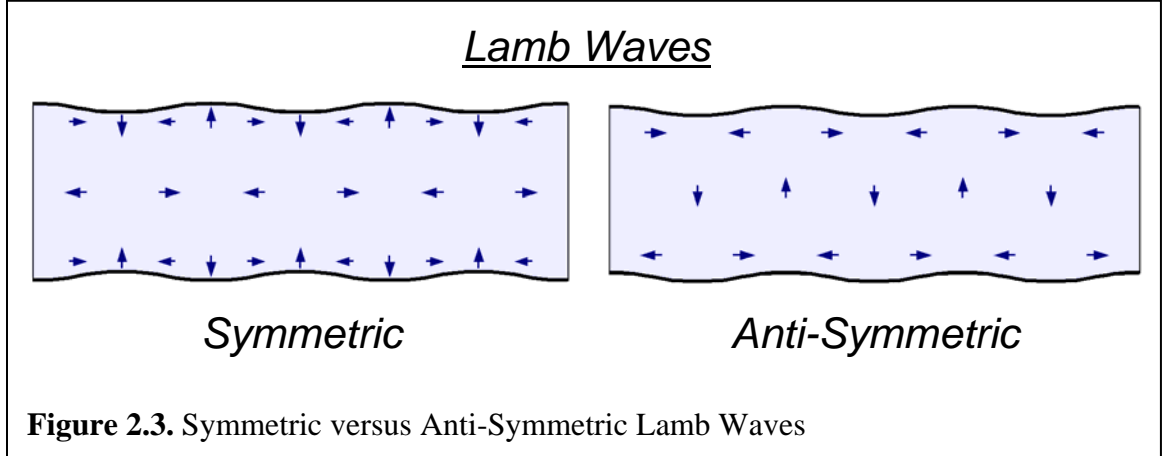
A subset of all surface acoustic wave polarizations, the Rayleigh wave is a common mode seen anywhere from resonators and sensors, to earthquakes traveling along the earth's surface. A Rayleigh wave has an elliptical polarization where the center of the rotation is located along the y-axis as seen in figure 2.1.



Ocean waves are similar to Rayleigh waves with the exception of the polarization of the elliptical particle displacement. While Rayleigh waves are polarized in the counterclockwise rotation, ocean waves possess a clockwise rotation and ultimately result in a different wave profile as seen in figure 2.2. The elliptical shape of the polarization is due to the fact that the air has lower impedance than the solid. This results in more displacement along the direction normal to the surface. [2]



The Rayleigh Wave itself is actually a combination of a longitudinal mode and a shear transverse mode propagating on an infinite substrate. If the substrate is not considered infinite, a Lamb Wave can develop. A Lamb wave occurs when the energy



from a Rayleigh Wave on one side of a substrate couples to the other side creating symmetric or anti-symmetric propagating waves (figure 2.3). For the experiments in this thesis the substrate is considered infinite because the thickness ($\sim 500 \text{ um}$) is an order of magnitude greater than the length of the acoustic wavelength ($\sim 10 \text{ um}$).

The characteristic equation used to relate the velocities of the longitudinal and shear components of a Rayleigh wave takes the form:

$$\left(\frac{V_R}{V_s}\right)^6 - 8\left(\frac{V_R}{V_s}\right)^4 + 8\left\{3 - 2\left(\frac{V_s}{V_l}\right)^2\right\}\left(\frac{V_R}{V_s}\right)^2 - 16\left\{1 - \left(\frac{V_s}{V_l}\right)^2\right\} = 0 \quad (2.1)$$

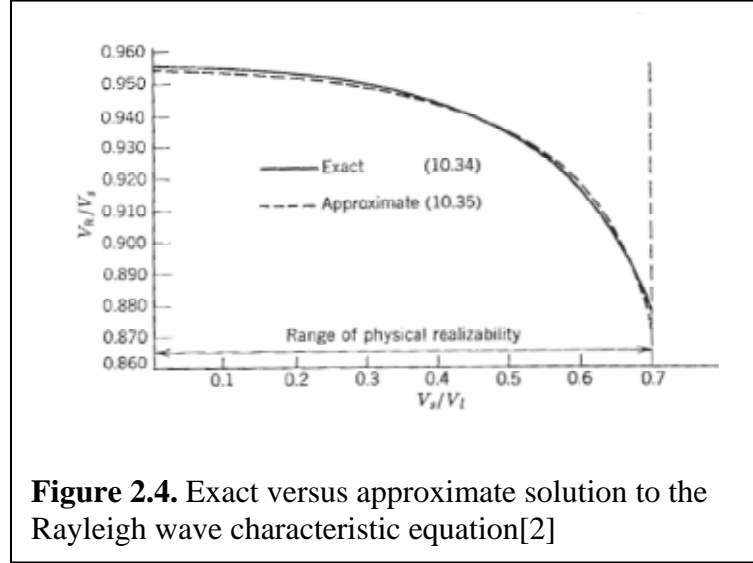
where V_s and V_l are the longitudinal and shear component velocities and V_R represents the Rayleigh velocity. V_R takes the form:

$$V_R = \frac{\omega}{\beta_R} \quad (2.2)$$

The solution for $\frac{V_R}{V_s}$ must be real and positive and therefore only one solution exists.

Figure 2.4 gives the solution as a function of the shear and longitudinal velocities in the substrate. This solution can also be approximated by using the formula:

$$\frac{V_R}{V_s} = \frac{0.87 + 1.12\sigma}{1 + \sigma} \quad (2.3), \quad \text{where } \sigma = \frac{1 - 2\left(\frac{V_s}{V_l}\right)^2}{2\left(1 - \left[\frac{V_s}{V_l}\right]^2\right)} \quad (2.4)$$



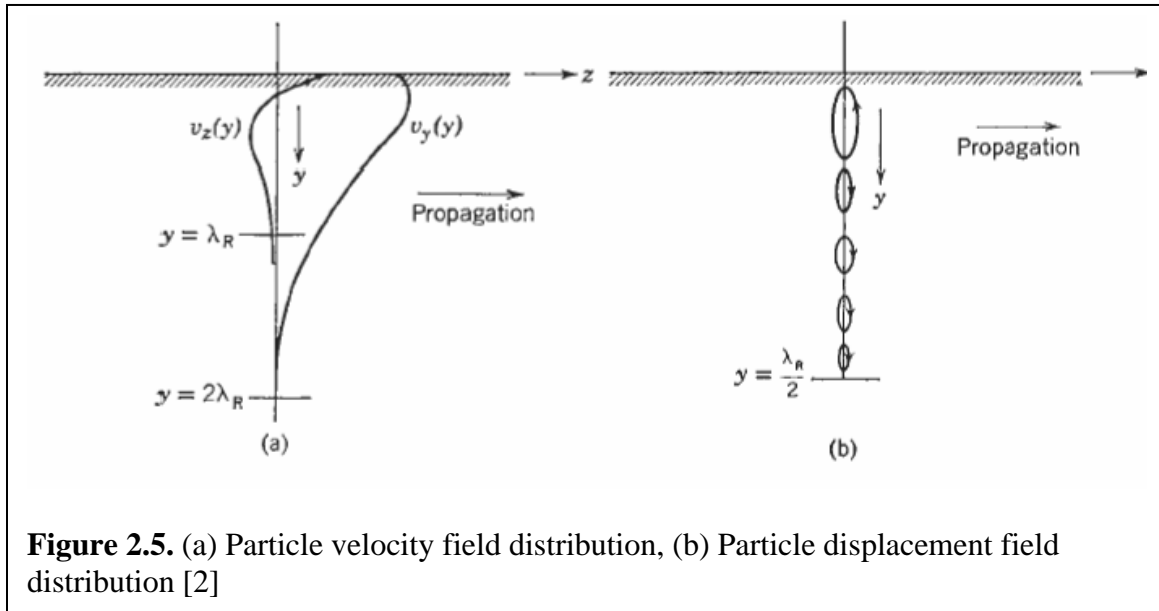
This figure shows how good of an approximation equation 2.3 is for estimating the solution to the Rayleigh wave characteristic equation. [2]

The field pattern for Rayleigh waves is shown in figure 2.5 below and clearly demonstrates how the energy of the wave decays going into the bulk. The partial velocity field is a combination of the longitudinal field partial wave and the shear field partial wave. The two partial wave velocity field patterns follow the equations:

$$v_y = \mp i\beta_R \left\{ e^{-\alpha_s y} - \frac{2\alpha_{fl}\alpha_{ts}}{\beta_R^2 + \alpha_{ts}^2} e^{-\alpha_{fl} y} \right\} e^{\mp i\beta_R z} \quad (2.4)$$

$$v_z = \alpha_{ts} \left\{ e^{-\alpha_s y} - \frac{2\beta_R^2}{\beta_R^2 + \alpha_{ts}^2} e^{-\alpha_{fl} y} \right\} e^{\mp i\beta_R z} \quad (2.5)$$

The particle displacement field distribution is elliptically polarized in the yz plane. Near the surface the Rayleigh wave motion is retrograde yet it reverses its sense at roughly a fifth of a wavelength into the bulk. Along with the varying polarization, the aspect ratio of the elliptical polarization varies with depth. [2]



2.2 Material Q Background

In general the quality factor is a figure of merit which attempts to measure the amount of energy saved per cycle divided by the amount of energy lost per cycle. This figure of merit is used across all fields of wave theory. Acoustic waves, like all waves, simply do not propagate with out any loss to the signal. If this were the case then Hooke's Law ($T = CS$) would be a precise equation requiring no modification for advanced calculations. Unfortunately, this is not the case due to viscous damping forces and nonlinearities within a solid and as a result Hooke's Law must be compensated to account for this. Equation 2.6 accounts for loss due to viscosity in Hooke's Law.

$$T = CS + \eta \frac{dS}{dt} \quad (2.6)$$

Viscosity is represented by η and has units of N s/m². The time derivative in the equation is due to the relaxation of strain as it settles toward equilibrium. [3]

The imperfect propagation of acoustic waves due to these damping forces and nonlinearities within the medium is measured by absorption. Absorption is the amount of energy lost versus the distance the wave has traveled. Derived in Rosenbaum [3] using the wave equation in 2.7 and complex wave number (equation 2.8), the expression for absorption takes the form seen in equation 2.9.

$$\rho \frac{\partial^2 v}{\partial t^2} = C \frac{\partial^2 v}{\partial z^2} + \eta \frac{\partial^3 v}{\partial t \partial z^2}, \quad (2.7)$$

$$\hat{k} = \frac{\omega}{v_a} + j\alpha, \quad (2.8)$$

$$\alpha = \frac{\omega \eta}{v_a^2 \rho} \left(\frac{\omega}{2v_a} \right) = \frac{\omega}{2Qv_a}, \quad (2.9)$$

In the above equations C is the stiffness constant, ρ is the density of the material, η is the viscosity of the material, and Q represents the material quality factor.

Material Q itself is defined as the ratio of the amount of energy stored versus the amount of energy lost per cycle [4]. More specifically the value for material Q can be calculated using the absorption coefficient, velocity, and frequency in equation 2.9.

$$Q = \frac{\omega}{2\alpha v_a} \quad (2.9)$$

Material Q varies over frequency and for homogenous material tends to be inversely proportional to frequency. This is because the absorption coefficient is proportional to the frequency squared. Typically in practice, the frequency dependence is ω^n , where $1.2 < n$

< 1.4 for poor quality materials and $n > 1.8$ for high quality materials. When $n < 1.7$ one can expect reduced absorption if the crystal growth conditions are improved. For heterogeneously layered materials the slope of the Q factor is less predictable as frequency changes. For anisotropic media material Q can also vary but usually no more than 5% to 10% over direction, however a notable exception to this is paratellurite (TeO_2) where the Q value can vary over orders of magnitude. [3]

In the case of acoustic resonators, material Q serves as the upper bound for the potential value of the resonator Q [7]. This means it is very important to know the material Q of the design materials ahead of time to ensure the resonator can be built with at least a certain Q value. I will now derive the equation for total resonator Q. To do so, the generalized definition for Q must be revisited. Equation 2.10 represents the energy lost divided by energy stored per cycle, where ω_0 is the frequency of the wave, E_s is the energy stored, and P_L is the energy loss rate.

$$Q = \frac{\omega_0 E_s}{P_L} \quad (2.10)$$

The first step in the derivation begins with considering all the different energy losses, including the loss due to the material, and losses due to the efficiency of the resonator in an ideal situation.

$$Q_{Total} = \frac{\omega_0 E_s}{(P_{LMaterial} + P_{LResonator} + \dots + P_{LN})} \quad (2.11)$$

By taking the inverse of both sides of the equation as in 2.12 and 2.13 it becomes possible to split each energy loss into its own term.

$$\frac{1}{Q_{Total}} = \frac{(P_{LMaterial} + P_{LResonator} + \dots + P_{LN})}{\omega_0 E_s} \quad (2.12)$$

$$\frac{1}{Q_{Total}} = \frac{P_{LMaterial}}{\omega_0 E_s} + \frac{P_{LResonator}}{\omega_0 E_s} + \dots + \frac{P_{LN}}{\omega_0 E_s} \quad (2.13)$$

Once each term is alone it becomes clear that each energy loss term is simply the inverse value for Q. Equation 2.14 accounts for not only the material and resonator Q values but any other loss mechanisms that may be accounted for within the system.

$$\frac{1}{Q_{Total}} = \frac{1}{Q_{Material}} + \frac{1}{Q_{Resonator}} + \dots + \frac{1}{Q_N} \quad (2.14)$$

Much like the equation for adding parallel resistive terms in electronic circuitry, the smallest Q value in the system dominates the total value for Q. Conversely, larger Q values tend to have less of an affect on the overall Q for the system. As a result of this, whenever the material Q is large in comparison to the other aspects of the system it plays a minor role in affecting the total Q value. If the material Q value is the smallest amongst the other Q values in the system it then dominates the entire system and the total Q can never be anything greater than the value of material Q.

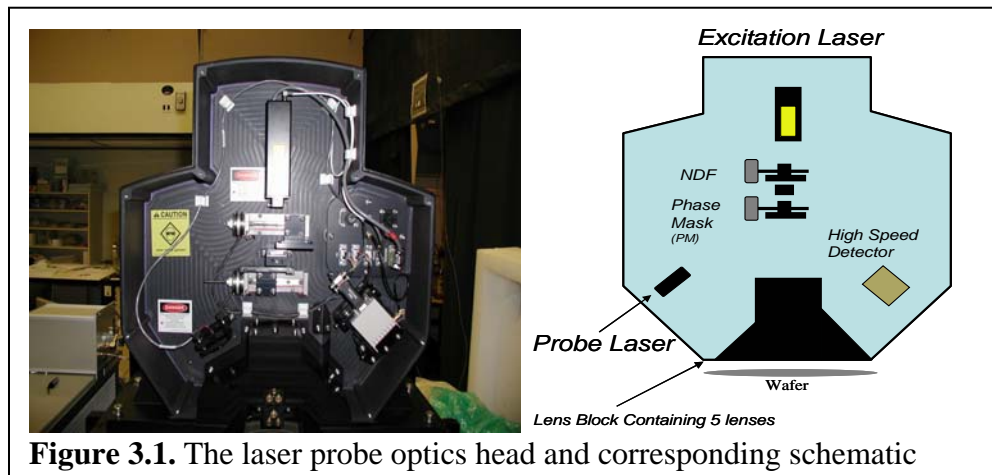
CHAPTER 3

THE LASER PROBE

This chapter will go into detail of the laser probe optics head design, the preparatory work done to bring it online, and the underlying physics of operation. The optics head of the laser probe is a very space efficient design and relies completely on transmissive components. The details of this design are discussed in the first section of this chapter. The original commercial laser probe included many features that were not necessary for our application; i.e. wafer handling. This led to only the principle components being donated to our lab including the optics head and the motor stage. The second section of this chapter will discuss the preparations, modifications, and software written we had to do to bring the entire laser probe system online. The last section of this chapter will explain, in detail, the physics behind the laser probe.

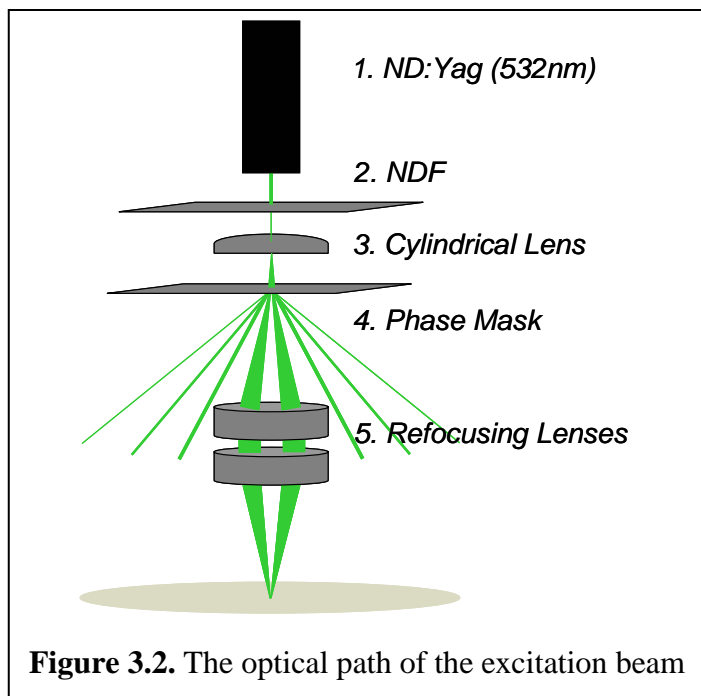
3.1 Laser Probe Design

The first version of the metrology tool was built very elegantly with consideration to the space the optical components took up. An image of the optics head is pictured on the left of figure 3.1 and a diagram for the system is pictured on the right side of the figure. This section will be broken down into the subsystems of the laser probe: the excitation beam, the probe beam and receiver, the camera view, and the motor control.



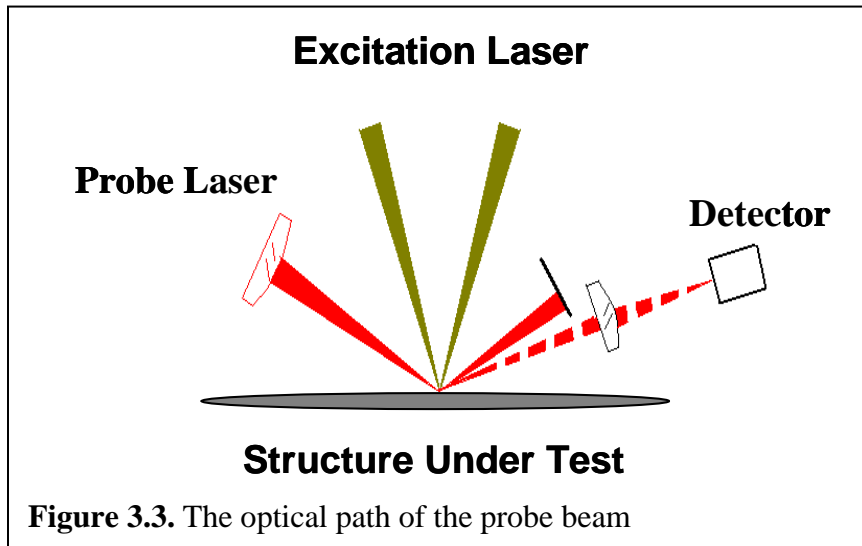
3.1.1 Excitation Beam

The excitation beam is generated by a ND:YAG laser which creates a beam with a wavelength of 1064 nm. The beam is pulsed with duration of ~100 picoseconds and is passively Q switched at 200 us. A frequency doubler is used on the excitation laser resulting in an actual wavelength of 532 nm. The excitation beam first travels through a neutral density filter in order to control the intensity of the beam on the surface. The attenuated light then passes through a cylindrical lens which elongates the beam. Next the excitation beam passes through a phase mask which diffracts the beam. The two first order diffracted beams are then passed through a set of lenses above the test wafer and refocused on the surface to create an interference pattern. The size of the interference pattern is ~300 microns thick and roughly a millimeter in the direction of the generated acoustic wave. The width of the pattern varies depending on which phase mask is used. Figure 3.2 is a diagram representing the path of the excitation beam through the optics head on the way to the device under test.



3.1.2 Probe Beam

The probe beam consists of a continuous wave AlGaAs IR diode laser with an optical wavelength of 808 nm. The probe beam is directed onto the surface of the device under test at a position incident to the excitation beam pattern. The spot size of the beam on the surface of the sample is roughly 100 microns. The acoustic waves generated by the excitation beam act as a diffraction grating for the IR probe beam. The probe light that is reflected from the surface is directed towards a stop while the diffracted light is aimed at a lens that directs the light toward the high speed detector. The detector utilizes a Silicon avalanche photodiode with a frequency range of 1 MHz up to 1 GHz. The photoreceiver outputs the signal to a LeCroy Oscilloscope which is in turn connected to the desktop computer. The schematic for the optical arrangement is depicted in Figure 3.3.



3.1.3 Motor Control, Laser Control, and Camera View

The stage motor control and the stepper motors in the optics system take full advantage of a CAN Open network. Five total amplifiers are used; three for the XYZ stage, one for the NDF stepper motor and one for the phase mask stepper motor. The

stage motors have a precision to a third of a micron allowing for reliable and precise targeting of the laser. The stepper motors within the optics system allow for fast NDF and phase mask setting changes. Whenever a certain phase mask or NDF setting is selected, the software tells the amplifiers to go to the preset locations. The CAN Open network also assists in the controls of the stage light and laser using a few of the pins on amp 4 that have been configured to act as outputs. The output sends a high signal to the Nanolase power supply which controls the pulsing of the laser.

The CCD camera focus is controlled by the Optem Zoom 100D optics set. Initially the system relied on a motor controlled focus lens set, however to save amplifiers a hand controlled optics Zoom 100D was selected. The image from the CCD is sent to the desktop computer and displayed in the control software.

3.2 Laser Probe Preparation

The components of the system that were donated include the motor stage, the optics head, and the nanolase power supply. The total value of the donated equipment came to \$180,000. To bring the system online more components were necessary. Power sources for the nanolase power supply, the photoreceiver, and CCD camera were introduced to the system. This DC power supply came from an old laser based experiment previously done in the MAG lab. Each motor also needed an amplifier to control it. The solution was found using a CAN Open amplifier network. These robust amplifiers are networked together and independently addressed. This allowed for improved simplicity when programming the software to control the system. The amplifiers were directly controlled by a desktop computer purchased solely for the operation of the laser probe.

Another important component for the system that was not donated to our lab was the control software. While this was initially an obstacle in the set up of the laser probe, the flexibility for software adaptation in later experiments came to be a strong advantage of our system. I developed the graphical user interface in LabView 8.0 and designed it to be capable of controlling virtually every aspect of the laser probe. Appendix B includes screen shots the GUI for the laser probe.

In the upper left corner of the interface are the relative position controls. The distance in micro steps are entered into the numeric input and the direction buttons move the stage the input distance in the selected direction. Each micro step corresponds to one third of a micron. Below the relative position controls are the absolute position controls. By entering in the coordinates of each axis and pressing GO, the motor stage will accurately position the laser over that location. Underneath the absolute position control are a few buttons that include control over the stage light, and lasers themselves. Control of the NDF and phase mask motors are done by selecting the position on the sliding index bar. Whenever a new position is selected the green light to the right of the bar comes on and the software will not respond to any other commands until the slide is in position. To the right of these controls is the camera image. The cross hairs in the middle of the image represent the location of the lasers being fired on the device under test. At the bottom of the GUI is the waveform as it is seen on the oscilloscope. The user can download the data from the oscilloscope onto the computer by selecting the “capture waveform” button. If the user wishes to store the downloaded waveform, he can do so but selected the save button next to the waveform.

The slowness curve controls are used to gather velocities over a range of frequencies from isotropic solids. This program relies on the aluminum wafer used to orient wafers over direction discussed in chapter five. To run the program the user must first input the start and finish angles as well as the increment size between angles. Then the software will prompt the user to move the aluminum plate to the correct starting angle. Once completed, the user clicks “OK” for the software to capture a waveform at that orientation. Once the capture is complete, the program prompts the user rotate the plate to the next angle and waits for the user to indicate completion. This cycle continues until all angles have been visited.

The dispersion curve button runs a script that prepares a set of waveforms from the phase masks selected by the array input. For each phase mask selected the laser probe will take a summed average of the waveform for 500 sweeps. After each averaged waveform has been downloaded onto the computer, the software saves all the data in a text file where all the odd columns correspond to the time axis of each waveform and all the even columns correspond to the amplitude axis of each waveform. A more detailed description of this program will be covered in chapter five.

3.3 Laser Probe Theory of Operation

This section will discuss why and how the laser probe works and how to interpret the resultant waveforms. This subsection will be broken into sections describing the optics of the excitation beam, acoustic generation by thermal expansion, and lastly interpretation of the data. The goal of this section is to give a general understanding of how the waves are being generated and measured.

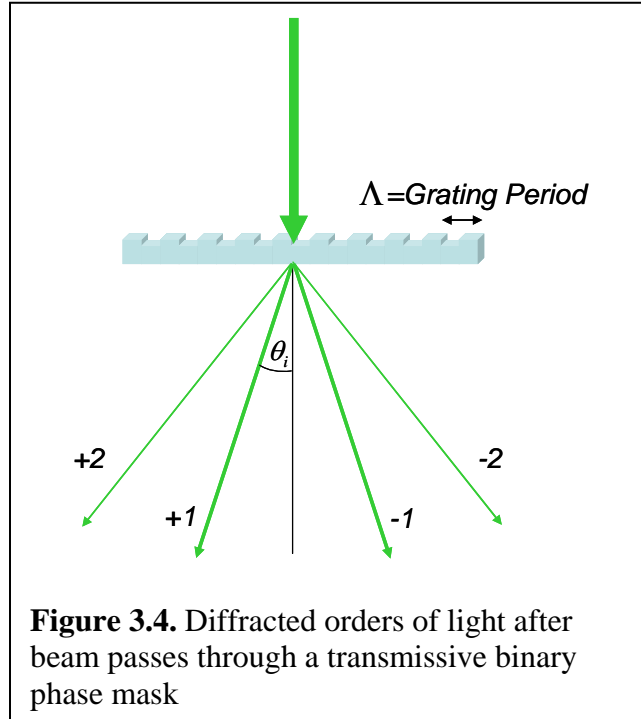
3.3.1 Excitation Beam Optics

The principle optical component of the laser probe itself is the transmissive phase mask along the path of the excitation beam. The purpose of this binary phase mask is to diffract the beam as it passes through the glass. Approximately 80% of the incident light is propagated into the +1 and -1 diffraction orders[8]. The angle of diffraction of the two first order beams diffracted through the phase mask follow the equation below:

$$\sin \theta_i = \sin \theta - i \frac{\lambda}{\Lambda \cdot n} \quad (3.1)$$

where θ_i represents the angle of diffraction for the i^{th} order, Λ represents the grating spacing, n is the index of refraction of the air around the phase mask and λ is the wavelength of the light[9]. Figure 3.5 is a diagram of the excitation pulse passing through the phase grating.

The angle that the two first order beams are diffracted from the phase mask is equal to the angle at which the two beams recombine on the test surface. Earlier designs of the laser probe relied on a reflective phase mask which took up a great deal more space. The transmissive grating allows for a much more space efficient design because no extra mirrors are necessary to direct the beams.



3.3.2 Acoustic Wave Generation

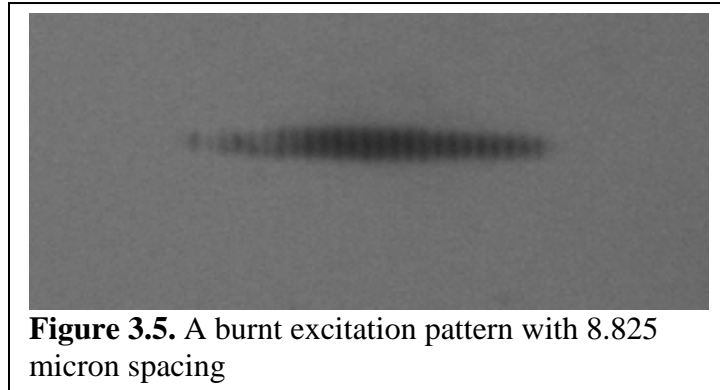
As the excitation beam recombines on the surface, an interference pattern is created. The spacing of this pattern follows the equation in 3.2 where Λ is the spatial period of the pattern, λ_e is the excitation wavelength, and θ is the angle of recombination.

[8]

$$\Lambda = \frac{\lambda_e}{2 \cdot \sin(\theta/2)} \quad (3.2)$$

Figure 3.6 is an example of what the spatial interference pattern looks like on the surface of the target. Provided the surface material has a strong enough emission frequency at the optical frequency of the excitation pulse, the excitation light can be absorbed. This absorption leads to a sudden, spatially periodic heating followed by thermal expansion. This thermal expansion results in the launching of counterpropagating acoustic waves.

The wave vector of these acoustic waves correlates to the spatial wavelength of the interference pattern. The ripple of the acoustic wave acts as a diffraction grating for the probe beam to interact with. The vertical displacement of this ripple due to the thermal absorption at the interference pattern is on the order of 100 nm [10, 11].

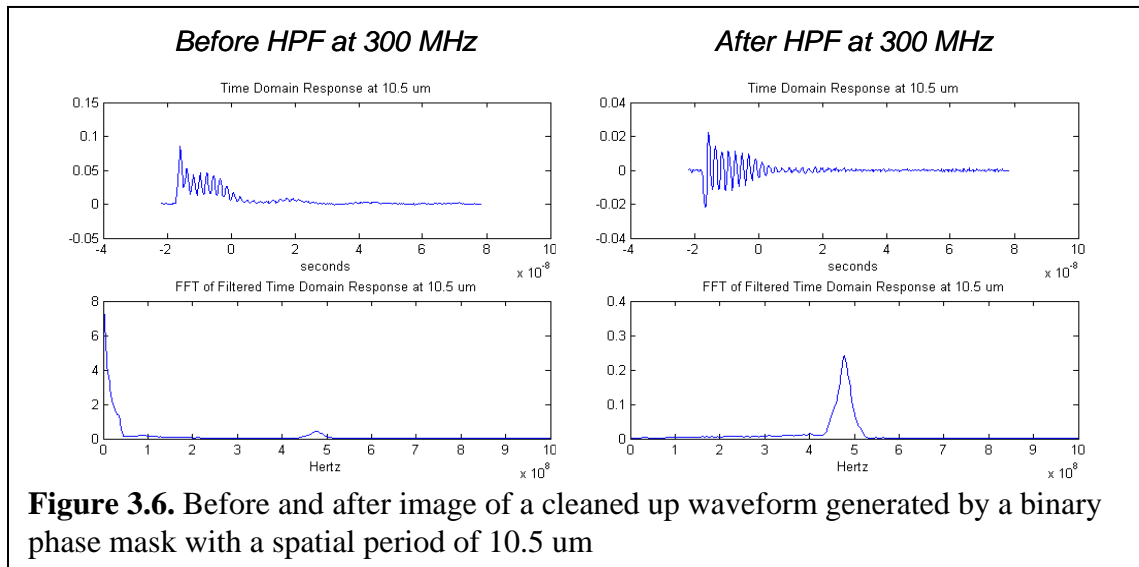


The waveforms acquired by the laser probe measurement technique carry a wealth of information. Along with the acoustic wave data, a low frequency component exists due to the slow decay of the surface displacement associated with the temperature grating. Coupling between the air above the surface of the material and the counterpropagating acoustic waves also create slow oscillations that show up in the resultant signal. The most prominent component of the signal, however, is from the high frequency counterpropagating waves. The two counterpropagating waves alone produce a modulation of the signal that is twice the acoustic frequency. A single acoustic wave, along with the static thermal grating, modulate the probe beam at exactly the frequency of the propagating acoustic wave. As long as the slowly decaying static thermal grating is present in the waveform, the measured acoustic frequency is accurate for the generated wave.[8, 10, 11]

3.3.3 Waveform Analysis

The waveform generated by the laser probe carries a wealth of information that can be analyzed to learn many characteristics of the material. A typical waveform, such as the one seen in figure 3.6, consists of a periodic dampened oscillation after an initial spike from thermal expansion. The decay of the total amplitude of the signal is from the surface displacement of the material over time. The oscillations within the envelope of the signal directly correspond to the frequency of the wave, which can be used to calculate the wave velocity if the wave vector is known. [8, 10, 11]

The ability to rapidly select a different phase mask allows for the generation of multiple waveforms for different acoustic k vectors in a short amount of time. This makes it very easy to create dispersion curves which can later be used for further calculations. By taking the fast Fourier transform of the signal it is easy to extract the frequency. The waveform must be cleaned up to obtain the frequency of the signal. Figure 3.6 shows before and after images of the cleaning process of the waveform.



It is clear from these diagrams that the low frequency components generated by thermal decay are sufficiently filtered out and the remaining acoustic data can freely be operated on.

CHAPTER 4

KRAMERS-KRONIG RELATIONS

The most essential part for the calculations of this experiment relies on the relationship known as the Kramers-Kronig relations. This relationship was first pioneered in the mid 1920s by Ralph Kronig and Hendrik Anthony Kramers to explain the absorption and dispersion in the X-Ray spectra [12, 13]. In essence, this pair of equations provides the ability to take dispersion data over a range of frequencies and calculate the corresponding set of attenuation data and vice versa. An analogous version to the Kramers-Kronig relationship used to describe optical waves has been developed [5, 6] to explain acoustic waves using the real and imaginary part of the dynamic compressibility. Like the optical counterpart, the acoustic version of this relationship requires the system to be both causal and linear.

Much like the original Kramers-Kronig relationship for optical systems, *a priori* information is required in order to translate imaginary or real data to its counterpart. In other words, for a given set of dispersion data to be converted to the attenuation data of the same frequency range, it is necessary to have information about the attenuation data ahead of time. For some applications, such as this experiment, the “anchor point” may not be known and a set of approximations are needed to circumvent the lack of information. The Kramers-Kronig relations are also a nonlocal relationship. In other words, in order for the attenuation to be calculated from the dispersion, the dispersion for all frequencies must be known. The approximations I have used in this thesis also approximate the Kramers-Kronig relationship locally. This section will first discuss the

origin and derivation of the Kramers-Kronig relationship and end with the derivation of the approximations used in this experiment.

4.1 Derivation of the Kramers-Kronig Relations

The original utility of the Kramers-Kronig relations was to relate the imaginary and real parts of the complex permittivity of an electromagnetic wave. This section will derive the Kramers-Kronig relationship based on the derivation found in the second edition of *Semiconductor Optoelectronic Devices* by Pallab Bhattacharya [14]. This derivation will begin with the complex dielectric constant of material for electromagnetic waves where the constant is given by:

$$\epsilon_r(\omega) = \epsilon'_r(\omega) + j\epsilon''_r(\omega) \quad (4.1)$$

In the time-invariant form the electric field \mathbf{E} and the electric flux density \mathbf{D} are related by

$$\begin{aligned} \mathbf{D} &= \epsilon_0 (1 + \chi^e) \mathbf{E} \\ &= \epsilon_r \epsilon_0 \mathbf{E} \end{aligned} \quad (4.2)$$

where χ^e is the electric *susceptibility*. Any temporal response of \mathbf{D} due to a change or switching of \mathbf{E} must include the change of polarization with time. The below expression expresses the causality relationship between the electric field and electric flux density.

$$\mathbf{D}(t) = \epsilon_0 \epsilon'_r \delta(t) \mathbf{E}(t) + \int_{-\infty}^t \epsilon_0 f(t-t') \mathbf{E}(t') dt' \quad (4.3)$$

This integral represents how the system at time t responds to the applied field at \mathbf{E} at a previous time t' . The Fourier transforms for both \mathbf{D} and \mathbf{E} are written as

$$\mathbf{D}(t) = \frac{1}{2\pi} \int_{-\infty}^{\infty} \mathbf{D}(\omega) e^{-j\omega t} d\omega \quad (4.4)$$

and

$$\mathbf{E}(t) = \frac{1}{2\pi} \int_{-\infty}^{\infty} \mathbf{E}(\omega) e^{-j\omega t} d\omega. \quad (4.5)$$

By substituting the Fourier transforms into the above causality relation one finds

$$\int_{-\infty}^{\infty} [\mathbf{D}(\omega) - \epsilon_0 (\epsilon'_\infty + f(\omega)) \mathbf{E}(\omega)] e^{-j\omega t} d\omega \quad (4.6)$$

with

$$f(\omega) = \frac{1}{2\pi} \int_{-\infty}^{\infty} f(t) e^{j\omega t} dt. \quad (4.7)$$

Because equation 4.6 must be valid for all values of t , the relation

$$\mathbf{D}(\omega) = \epsilon_0 (\epsilon'_\infty + f(\omega)) \mathbf{E}(\omega) \quad (4.8)$$

is valid between the Fourier components, so that

$$\epsilon_r(\omega) = \epsilon'_\infty + \frac{1}{2\pi} \int_{-\infty}^{\infty} f(t) e^{j\omega t} dt \quad (4.9)$$

$$= \epsilon'_\infty + f(\omega) \quad (4.10)$$

The *Cauchy principle value theorem* can be shown as

$$P \int_{-\infty}^{\infty} \frac{f(\omega') d\omega'}{\omega' - \omega} - j\pi f(\omega) = 0 \quad (4.11)$$

where P represents that the principle value of the integral. The second part of the above equation represents the infinitesimally small semi-circle about the simple pole $\omega' = \omega$.

The contour integrated over by the *Cauchy principle value theorem* is shown in figure 4.1

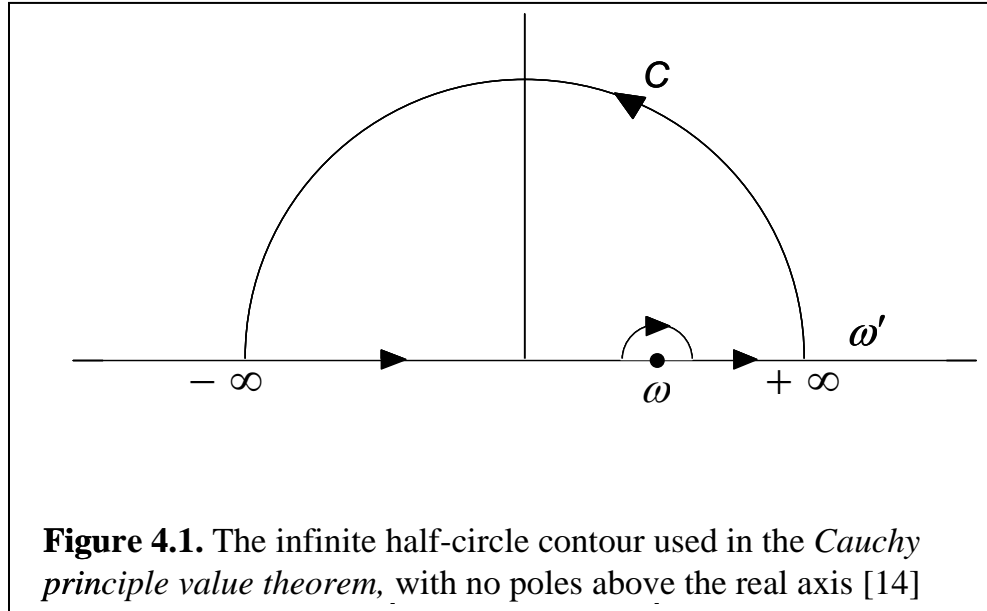
From equation 4.11, by application of the Cauchy theorem to the function

$[\epsilon'_r(\omega) - \epsilon'_\infty] / (\omega' - \omega)$, the following relations can be derived.

$$\epsilon'_r(\omega) = \epsilon'_\infty + \frac{2}{\pi} P \int_0^\infty \frac{\omega' \epsilon''_r(\omega) d\omega'}{\omega'^2 - \omega^2} \quad (4.12)$$

$$\epsilon_r''(\omega) = -\frac{2}{\pi} P \int_0^{\infty} \frac{[\epsilon_r'(\omega') - \epsilon_{\infty}'] d\omega'}{\omega'^2 - \omega^2} \quad (4.13)$$

These integrals are the Kramers-Kronig relations for the complex permittivity of material.



4.2 Derivation of the Kramers-Kronig Approximations for Acoustic Applications

Acoustic wave theory and optical wave theory are analogous in the governing equations. Figure 4.2 compares the one-dimensional acoustic equations to Maxwell's equations for both the fundamental physical laws and the constitutive relations.

<i>One-Dimensional Acoustic Equations</i>	<i>Maxwell Equations</i>
FUNDAMENTAL PHYSICAL LAWS	
$\frac{\partial T}{\partial z} = \rho \frac{\partial v}{\partial t}$ Newton's law	$\nabla \times \mathbf{E} = -\frac{\partial \mathbf{B}}{\partial t}$ Faraday's law
$S = \frac{\partial u}{\partial z}$	$\nabla \times \mathbf{H} = \frac{\partial \mathbf{D}}{\partial t} + \mathbf{J}$ Ampere's law
CONSTITUTIVE EQUATIONS	
$T = CS$ Hooke's law	$\mathbf{D} = \epsilon \mathbf{E}$
$v = \frac{\partial u}{\partial t}$	$\mathbf{B} = \mu \mathbf{H}$

Figure 4.2. A comparison between the common acoustic and optical governing equations [3]

From the table it is worth noting how the stiffness constant C is analogous to the electromagnetic permittivity. The compressibility K is the inverse of the stiffness constant. For the Kramers-Kronig relationship for acoustic waves the real and imaginary parts of the compressibility are used and the relationship can be defined as

$$K_1(\omega) = K_1(\infty) + \frac{2}{\pi} P \int_0^{\infty} \frac{\omega' K_2(\omega')}{\omega'^2 - \omega^2} d\omega' \quad (4.14)$$

$$K_2(\omega) = -\frac{2}{\pi} P \int_0^{\infty} \frac{\omega K_1(\omega')}{\omega'^2 - \omega^2} d\omega' \quad (4.15)$$

where K_1 and K_2 are the real and imaginary part of the adiabatic compressibility of a medium. This relationship has been verified by various researchers studying the properties of acoustic waves [5, 6, 15]. The remainder of this section will derive the approximation equations used in this experiment; the derivation will come from the M. O'Donnell, E. T. Jaynes, and J. G. Miller paper published in the *Journal for the Acoustical Society of America*[5].

The compressibility of an acoustic wave is related to the wavenumber of that wave by

$$k^2 = \omega^2 \rho_0 K(\omega) \quad (4.16)$$

where k is the wavenumber and ρ_0 is the density of the medium. The complex wavenumber is expressed as

$$\hat{k} = \frac{\omega}{C(\omega)} + j\alpha(\omega) \quad (4.17)$$

where C is the phase velocity and α represents the absorption coefficient. The compressibility can be related to the absorption and phase velocity by substituting equation 4.17 into equation 4.16 yielding

$$\frac{\omega^2}{C^2(\omega)} - \alpha^2(\omega) + \frac{2i\omega\alpha(\omega)}{C(\omega)} = \omega^2 \rho_0 [K_1(\omega) + iK_2(\omega)]. \quad (4.18)$$

By separating the imaginary and real components of the previous equation one yields

$$\frac{\omega^2}{C^2(\omega)} - \alpha^2(\omega) = \omega^2 \rho_0 K_1(\omega) \quad (4.19)$$

and

$$\frac{2\alpha(\omega)}{C(\omega)} = \omega \rho_0 K_2(\omega). \quad (4.20)$$

These equations decouple for the usual case in which the magnitude of the imaginary part of the wavenumber is much less than the magnitude of the real part

[i.e., $\alpha(\omega)C(\omega)/\omega \ll 1$] for all frequencies. The decoupled equations that relate K_1

with $C(\omega)$, and K_2 with $\alpha(\omega)$ can be written as

$$C(\omega) = 1/[\rho_0 K_1(\omega)]^{1/2} \quad (4.21)$$

$$\alpha(\omega) = [\rho_0 C(\omega)/2] \omega K_2(\omega) \quad (4.22)$$

Equations 4.14, 4.15, 4.21, and 4.22 allow for a complete relationship between the attenuation coefficient and phase velocity in the frequency domain. Unfortunately, this relationship is non local since the computation of one variable necessitates knowledge of the complementary variables for all frequencies.

The next part of this derivation will rely on the analogy between the acoustic Kramers-Kronig relation and the relationship between the frequency dependence of the gain and phase shift of an electrical amplifier. This relationship will allow for the derivation of the approximation over a small frequency range in a non resonant system. Bode demonstrated that at any frequency, the phase shift is directly related to the change in amplitude over frequency [16]. Provided the system exhibits no resonances, the

approximation is very accurate over a limited frequency range centered at the frequency of interest. The derivation of this similar approximation for attenuation and phase velocity begins with equation 4.15 and by implementing a change of variable $x = \ln(\omega' / \omega)$ to evaluate the integral. The imaginary part of the compressibility becomes

$$K_2(\omega) = -\frac{2}{\pi} \int_{-\infty}^{\infty} \frac{G(x) - G(\infty)}{e^x - e^{-x}} dx \quad (4.23)$$

where $G(x) = K_1(\omega')$ and $G(\infty) = K_1(\infty)$ since x is infinite for ω' equal to infinity. Using integration by parts, the imaginary component of compressibility reduces to

$$K_2(\omega) = -\frac{2}{\pi} \int_{-\infty}^{\infty} \frac{dG(x)}{dx} \ln \coth\left(\frac{|x|}{2}\right) dx. \quad (4.24)$$

From the behavior of the function $\ln \coth(|x|/2)$ seen in figure 4.2 the above equation can be cast into an approximate local form. The sharp singularity around the point $x=0$ causes the magnitude of the integral to be dominated by the value of $x=0$. The integral is now rewritten as

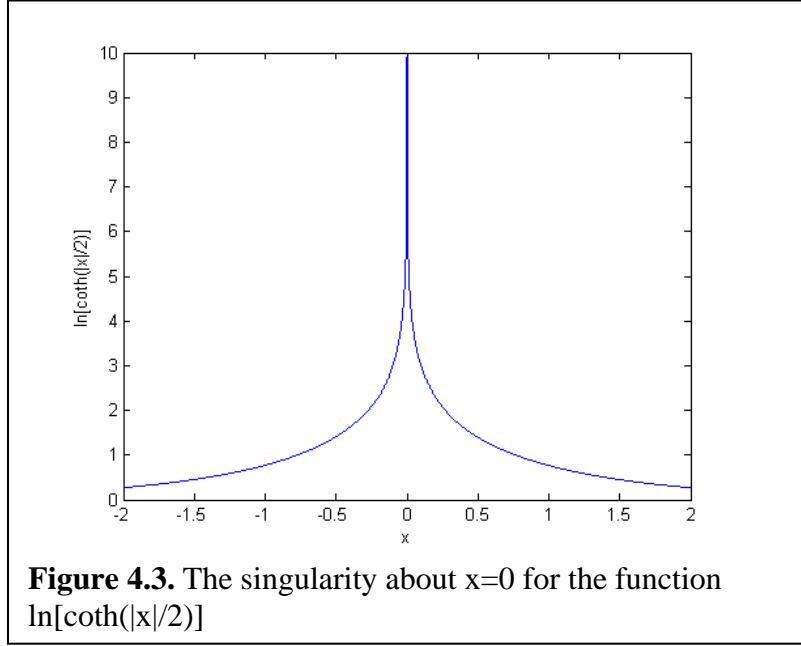
$$K_2(\omega) = -\frac{1}{\pi} \int_{-\infty}^{\infty} F(x) \ln \coth\left(\frac{|x|}{2}\right) dx, \quad (4.25)$$

where $F(x)$ is equal to $dG(x)/dx$.

An approximation to integral 4.25 can be found by expanding $F(x)$ about $x = 0$. The integral can further be rewritten as

$$K_2(\omega) = -\frac{2}{\pi} \sum_{n=0}^{\infty} \frac{F^{2n}(0)}{(2n)!} \int_0^{\infty} x^{2n} \ln \coth\left(\frac{|x|}{2}\right) dx, \quad (4.26)$$

because the function $\ln \coth(|x|/2)$ is even and the odd powers of x in the expansion vanish. The $F^{2n}(0)$ term in equation 4.26 corresponds to the $2n$ th derivative of $F(x)$ evaluated at $x=0$.



The next step of the derivation is expanding $\ln \coth(|x|/2)$ in powers of e^{-x} to obtain

$$K_2(\omega) = -\frac{4}{\pi} \left[\sum_{n=0}^{\infty} F^{2n}(0) \left(\sum_{m=0}^{\infty} \frac{1}{(2m+1)^{2n+2}} \right) \right]. \quad (4.27)$$

This expression shows how K_2 is related to the sum of the even derivatives of $F(x)$ evaluated at $x = 0$. So long as both the phase velocity and attenuation coefficients are slowly varying in terms of frequency, the equation 4.27 can be approximated by the first few terms. Equations 4.28 and 4.29 represent the equation in 4.27 under these conditions.

$$K_2(\omega) = -\frac{4}{\pi} \left(\frac{\pi^2}{8} F(0) + \frac{\pi^4}{96} F''(0) + \dots \right) \quad (4.28)$$

Substituting for $F(x)$ yields

$$K_2(\omega) = -\frac{\pi}{2} \left. \frac{dG(x)}{dx} \right|_{x=0} - \frac{\pi^3}{24} \left. \frac{d^3G(x)}{dx^3} \right|_{x=0} + \dots \quad (4.29)$$

The component $dG(x)/dx$ is related to the dispersion, $dC(\omega)/d\omega$, and evidence to this will be provided below. The higher derivatives of $G(x)$ also correspond to the higher derivatives of the phase velocity in the frequency domain. As long as the change of dispersion is small over a limited frequency range, the higher order derivatives can be neglected. When the first order derivative dominates, the higher order terms can be neglected and the leading term in equation 4.29 can be written as

$$\left. \frac{dG}{dx} \right|_{x=0} = \frac{dK_1(\omega)}{d\omega} \left. \frac{d\omega}{dx} \right|_{x=0} = \omega \frac{dK_1(\omega)}{d\omega}, \quad (4.30)$$

and $K_2(\omega)$ becomes

$$K_2(\omega) = -\frac{\pi}{2} \omega \frac{dK_1(\omega)}{d\omega}. \quad (4.31)$$

This last equation relates the imaginary component of the compressibility at a given frequency to the local rate of change of the real component at the same frequency.

Looking at equation 4.21, which relates the phase velocity to the real component of the compressibility, the derivative of $K_1(\omega)$ in the frequency domain becomes

$$\frac{dK_1(\omega)}{d\omega} = -\frac{2}{\rho_0 C^3(\omega)} \frac{dC(\omega)}{d\omega} \quad (4.32)$$

Now equation 4.32 can be combined with equation 4.31 and 4.22 so that $dC(\omega)/d\omega$ becomes

$$\frac{dC(\omega)}{d\omega} = 2C^2(\omega)\alpha(\omega)/\pi\omega^2, \quad (4.33)$$

and $\alpha(\omega)$ becomes

$$\alpha(\omega) = \frac{\pi\omega^2}{2C^2(\omega)} \frac{dC(\omega)}{d\omega}. \quad (4.34)$$

Equation (4.33) can be rewritten as

$$\frac{dC(\omega)}{C^2(\omega)} = \frac{2\alpha(\omega)}{\omega^2} d\omega, \quad (4.35)$$

in order to integrate both sides from some reference frequency ω_0 to ω . By doing this, the phase velocity can be related to the attenuation coefficient according to the expression

$$\frac{1}{C_0} - \frac{1}{C(\omega)} = \frac{2}{\pi} \int_{\omega_0}^{\omega} \frac{\alpha(\omega')}{\omega'^2} d\omega', \quad (4.36)$$

where C_0 is the sound velocity at ω_0 . Equations 4.34 and 4.36 represent nearly localized approximations relating the attenuation coefficient and the phase velocity. The magnitude of the dispersion is usually small; therefore these equations can be further simplified to

$$\alpha(\omega) = \frac{\pi\omega^2}{2C_0^2} \frac{dC(\omega)}{d\omega}, \quad (4.37)$$

$$\Delta C = C(\omega) - C_0 = \frac{2C_0^2}{\pi} \int_{\omega_0}^{\omega} \frac{\alpha(\omega')}{\omega'^2} d\omega' \quad (4.38)$$

where $C(\omega)$ is written as $C_0 + \Delta C(\omega)$ with $\Delta C(\omega) \ll C_0$, and only terms of order $\Delta C(\omega)$ are retained. For calculations used in this experiment, equation 4.37 is the only necessary approximation needed. Equation 4.37 is applied to each point of the dispersion curve generated by the laser probe data in order to generate an attenuation coefficient curve over the same range of frequencies. This attenuation curve can then be used in conjunction with the dispersion to calculate Material Q as seen in equation 1.2.

CHAPTER 5

EXPERIMENTAL PROCEDURE

This chapter will outline the experimental method I have developed to measure material Q over frequency. The first section will discuss the preparation of the wafer and the laser probe so that acoustic data can be measured by the probe. The second section walks through how to acquire data using the laser probe and describes how the dispersion curve acquisition software works. The last section will present the software I have written along with Ryan Westafer, to extract the necessary data from the measured waveforms. It will also discuss the other software program I have written which applies the Kramers-Kronig approximations to calculate the attenuation and ultimately material Q.

5.1 Experimental Preparation

Once a material is selected to be characterized by the laser probe, preparation of the material for excitation beam absorption is essential. If the absorption spectrum of the material is known to be very strong for 532 nm green light, no extra preparation is needed. If the test material poorly absorbs 532 nm light a thin layer of copper should be evaporated onto the surface of the wafer. The thickness of the copper should be something that is acoustically thin enough to have a minimal effect on the Rayleigh waves of the substrate, yet optically thick enough to absorb a significant amount of green light to generate a thermal grating. We have found ~100 nm of copper to be a suitable thickness. Once the copper layer is evaporated on the surface of the test material, the material should be lined up on the aluminum plate. The aluminum plate is 8.5 inches in diameter and has straight lines etched perpendicular to each other. These lines are used to line up the flats of a wafer in a given direction so the experimenter has more precise

